Chapter-3

Exploration of Auxochromic Properties of Ring-Fused Azacyclic Groups and their application

3. Exploration of Auxochromic Properties of Ring-Fused Azacyclic Groups and their Application

3.1. Coumarin-Fused-Azacyclic Group: Synthesis, Photophysical Properties and Cellular Compatibility Studies

3.1.1. Background and Rationale

Since their inception, fluorophores have undergone continual chemical modification to impart desired photophysical and physicochemical characteristics, such as fluorogenicity, water solubility, cell membrane permeability, as well as resilience to photobleaching.[1,2] Despite persistent efforts, the development of an ideal fluorophore may appear challenging. Over the past decade, researchers have definitively identified several crucial auxochromes that can precisely modulate the physicochemical and fluorogenic characteristics of established small molecule fluorophores. This can be best explained with the following example of aminocoumarins (figure. 3.1). The substitution of the 7th position dimethylamine or diethylamine of coumarin (**1a-1b**) with an azetidine or aziridine ring (**2a-2b**) significantly enhances the fluorescence quantum yield (ϕ_f) of the core scaffold (Fig. 3.1a).[3,4] Further modification of azetidine to azaspirocyclic (**3a-3b**) and azaspiroketal rings (**4a**) helps to balance the solubility and permeability of the coumarin core.[5,6] During the period between 1970 - 1990s, a considerable number of annulated azacoumarins, such as tetrahydropyrido-4-methylcoumarin (**5**), 4',5'-dihydropyrrolo-4-methylcoumarin (**6**) and 4-methylpyranocarbazole (**7**), were synthesized for use as emission sources for dye laser applications. The investigation of these molecules has been exclusively focused on their synthetic pathways and restricted to evaluation of basic photophysical parameters (absorption and emission maximum, quantum yields, etc.) without delving much into their fluorogenic applications.[7–9] We are driven by our keen interest as fluorophore developers[11] to extensively explore these annulated azacoumarin systems and fully understand their potential in developing

fluorescent probes (figure 3.1b). In this chapter, we present the synthesis and photophysical characterization of these azacoumarins.

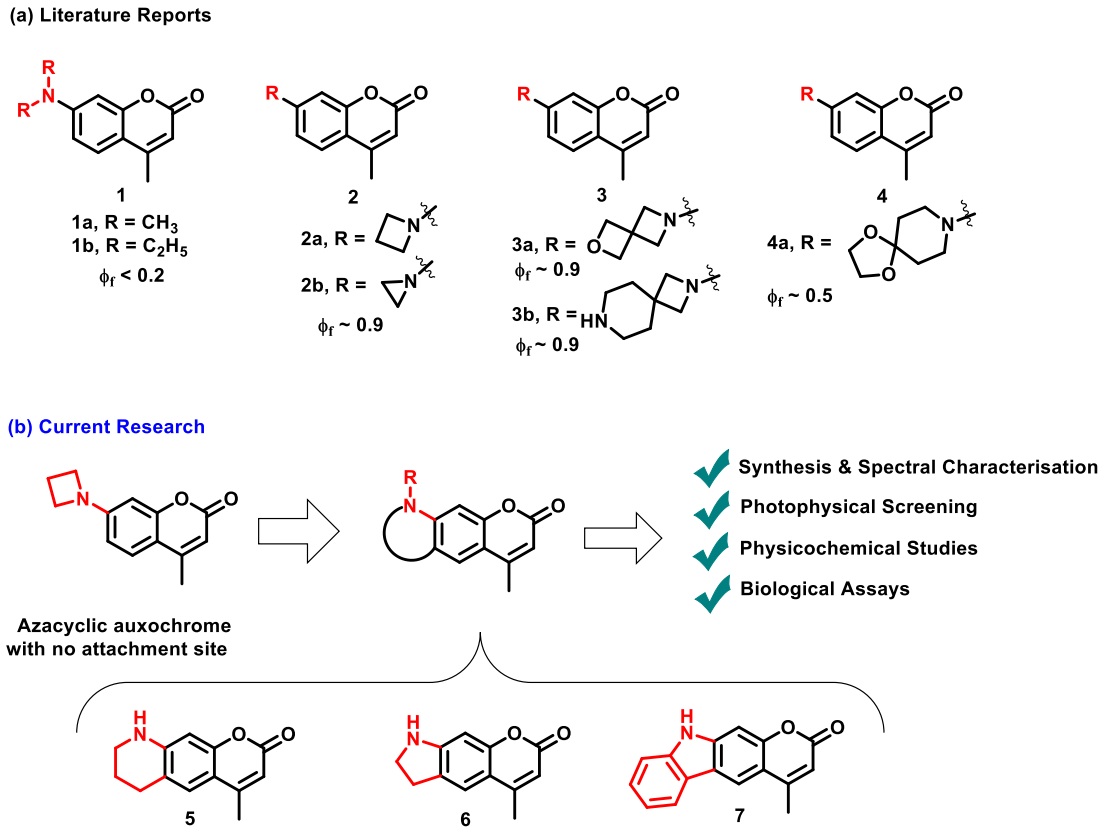

Figure 3.1. (a)The gradual advent of novel auxochromes reported in the literature; and (b) Demonstration of objectives of current work.

3.1.2. Results and discussion

3.1.2.1. Synthesis of target molecules

The target structures (**5-7**) were obtained using the synthetic routes outlined in scheme 3.1.[7,9,10] The synthetic methods involve the use of Pechmann condensation with ethyl acetoacetate in the presence of a Lewis acid, $ZnCl_2$ (in case of **5** and **6**) or conc. H_2SO_4 (cat.) (in case of **7**) affording the desired compounds in variable yields (55-75%). Additionally, to study the impact of alkyl substitution on the photophysical properties of these compounds, molecule **5** was subjected to *N*-methylation to generate **5a** in 50% yield.

Scheme 3.1. Synthesis of azacoumarin derivatives 5, 5a, 6 and 7.[a]

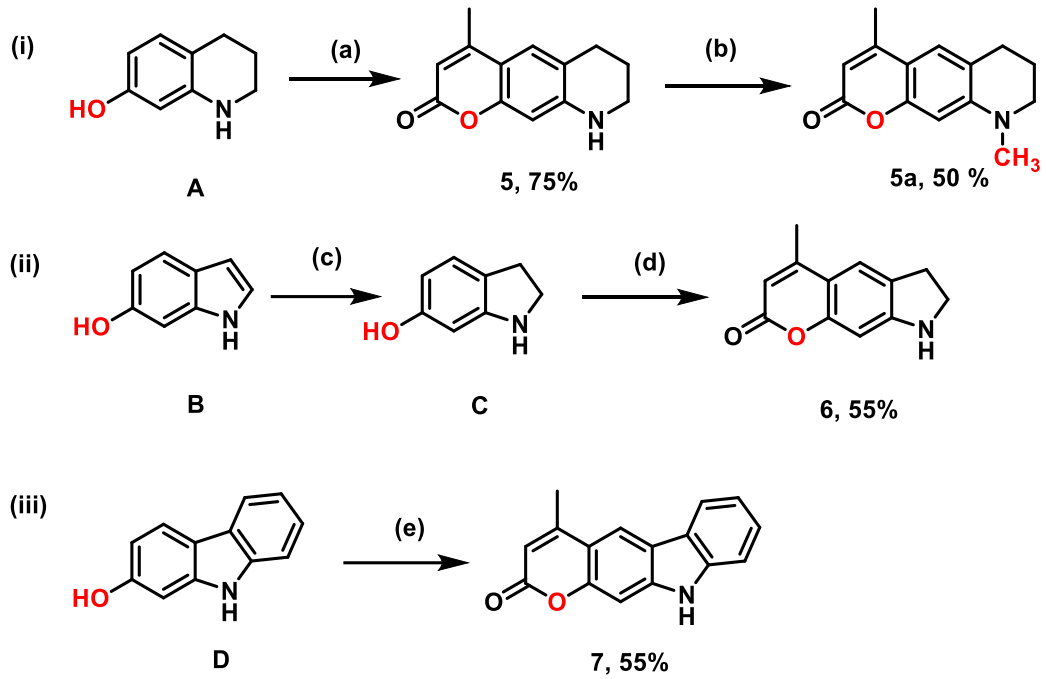

[a]**Reagents and Conditions.** (a) **A** (2.01 mmol), $ZnCl_2$ (1.5 equiv.), ethyl acetoacetate (1.2 equiv.), EtOH, reflux at 85 - 90 °C for 16 h; (b) 5 (0.96 mmol), CH_3I (1.5 equiv.), K_2CO_3 (1.5 equiv.), ACN, 65 °C, heat for 6 h; (c) **B** (1.48 mmol), $NaBH_3CN$ (3 equiv.), AcOH (0.5 mmol), rt, 2h, 78%; (d) **C** (2.22 mmol), $ZnCl_2$ (1.5 equiv.), ethyl acetoacetate (1.2 equiv.), EtOH, reflux at 85 - 90 °C for 16 h; (e) **D** (1.63 mmol), H_2SO_4 (0.2 mL), ethyl acetoacetate (1.2 equiv.), EtOH, reflux at 85 - 90 °C for 16 h. [b]Isolated yields.

3.1.2.2. Photophysical characterization of molecules.

The synthesized compounds **5-7** were thoroughly analysed for their photophysical properties which included absorption and emission maxima in PBS, Stokes' shift, molar absorptivity (ε), quantum yield and brightness (Table 3.1), with compound **2a** serving as the reference standard. The absorption maxima (λ_{abs}) for compounds **5-7** and **2a** in phosphate buffer saline (PBS) were recorded at 359-378 nm and 355 nm, respectively (Table 3.1, Figure 3.2). The fluorescence emission maxima for compounds **5-7** were recorded at 456-464 nm, which is closely aligned with the standard **2a** (λ_{em}= 478 nm) (Table 1, Figure 3.2). Notably, compound **5a** (*N*-methyl derivative of **5**) demonstrated a bathochromic shift in both absorption and emission maxima,

while maintaining a similar Stokes' Shift compared to **5**. Even though there was a notable increase in the molar absorptivity value of **5a** compared to **5**, there was a significant drop in the ϕ_f for **5a**. Reduction in annulated ring size from six-membered (**5**) to five-membered (**6**) blue-shifted both absorption and emission wavelengths. The reduction in ring size led to a slight increase in the Stokes' shift and a drastic elevation of the molar absorptivity, but a decrease in the quantum yield was observed. Furthermore, the incorporation of a carbazole ring into the coumarin scaffold, as seen in **7**, led to a large Stokes' shift but compromised the molar absorptivity, as well as, the ϕ_f on the other hand. Based on the calculated brightness index, compound **6** displayed the highest fluorescence brightness (~17000), surpassing reference **2a** (~11000). As a result, compound **6** has been prioritized for extensive physicochemical studies to assess its potential as a fluorescent probe.

Table 3.1. Photophysical properties of compounds 5, 5a, 6 and 7.

Comp. no.	λ_{abs} (nm)[a]	λ_{em} (nm)[b]	Stokes' Shift (nm)	ε[c] (M^{-1} cm^{-1})	ϕ[d]	Brightness (M^{-1} cm^{-1})
5	378	459	81	6458	0.901	5818
5a	383	465	82	14920	0.779	11622
6	359	456	97	22370	0.760	17001
7	362	464	102	5217	0.095	495
2a	355	478	123	12100	0.935	11320

[a]λ_{abs} = absorbance maximum in PBS; [b]λ_{em} = emission maximum in PBS; [c]Molar absorptivity in PBS; [d]Quantum yield in PBS.

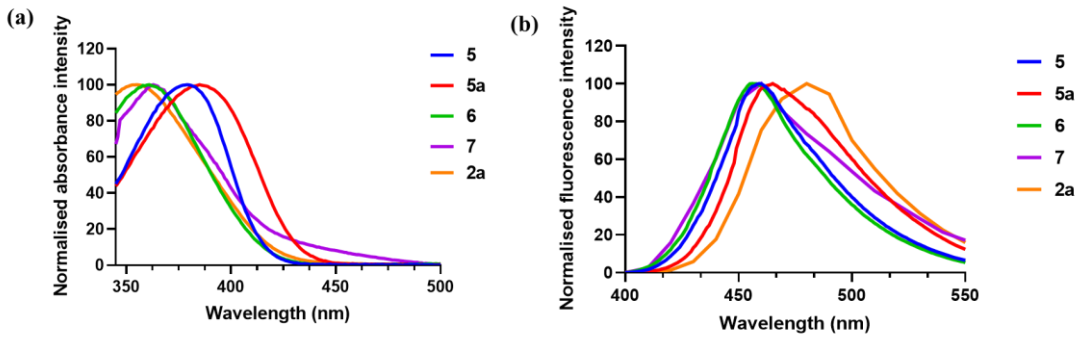

Figure 3.2. (a) Normalised absorbance intensities and (b) normalised fluorescence emission intensities of compounds **5-7** in PBS.

3.1.2.3. Physicochemical Characterization of Compound 6

Compound **6** underwent further testing to assess its pH stability and photostability. Compound **6** showed no significant changes in its fluorescence emission intensity (figure 3.3a) over the physiological pH range (4-7), thus confirming its stability. The photostability of dyes is an essential parameter for their bioimaging applications. Evaluation of the photostability of compound **6** was conducted in comparison to azetidinylated counterpart **2a** by a time-dependent photobleaching method using a well-known cell-labelling dye coumarin **6** (λ_{ex}: 457 nm; λ_{em}: 501 nm) as the reference standard. For the photostability study, the compounds **6**, **2a** and coumarin **6** were dissolved in DMSO/PBS (20:80) and subjected to continuous irradiation with a 500W tungsten lamp emitting white light. The emission intensities were measured from 0 to 360 minutes. The results indicated that the photostability of compound 6 is comparatively better than that of the azetidinylated derivative **2a** (figure 3.3b).

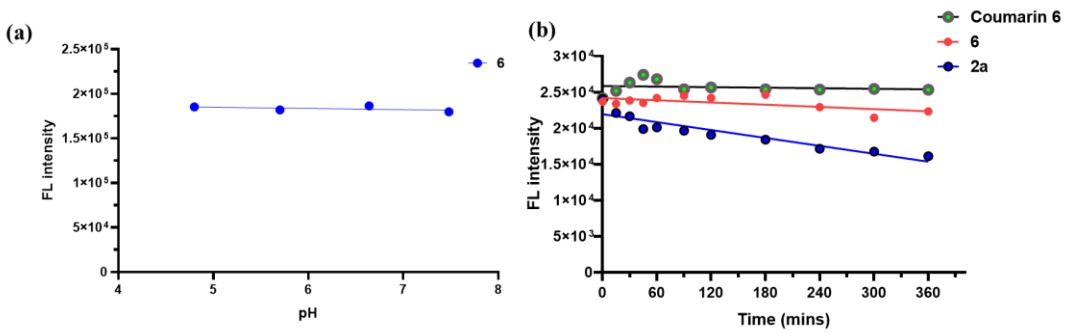

Figure 3.3. (a) pH stability study of compound **6** in a pH range of 4-8, and (b) Photostability study of compound **6** measured in terms of change of fluorescence intensity in comparison to **2a** and **coumarin 6** with time (0 – 360 minutes).

3.1.2.4. Biocompatibility assay of Compound 6

Delighted with the substantial pH stability and extended photostability of compound 6, we then proceeded to investigate its biocompatibility in both cancer (MCF-7) and normal (HEK-293) cell lines. Compound 6 exhibited over 90% cell viability below 50 μM concentration in MCF-7 cell line (figure 3.4a), and over 80% cell viability even at a concentration as high as 100 μM in HEK-293 cells (figure 3.4b). Hence, it can be safely used for bioimaging purposes in both cancer and normal cell lines. Moreover, the uptake of compound **6** by living MCF-7 cells was quantitatively determined using flow cytometry revealing an almost 80% enhancement in the fluorescence intensity compared to the control, confirming excellent cellular permeability of the fluorophore (figure 3.5).

Compound **6** fulfills all the requirements of a desired fluorophore, including high brightness, a decent Stokes' shift, stability within the physiological pH range (4-8), significant photostability, low cytotoxicity, and good cell permeability. Additionally, it features a free nitrogen centre for attaching a response unit. Consequently, we aimed to convert compound 6 into a fluorescent

probe to demonstrate the use of azacyclic auxochromes in the development of modern fluorescent probes.

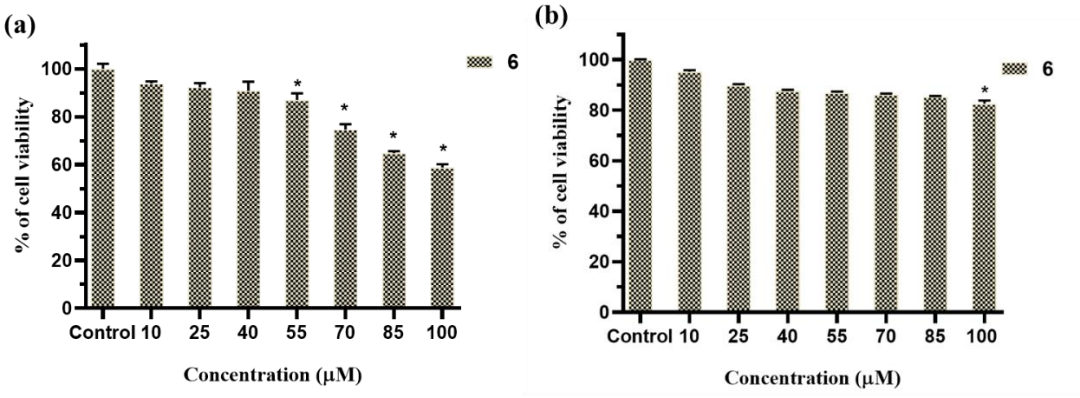

Figure 3.4. (a) Measurement of percentage of viability of MCF-7 cells incubated with compound **6** at various concentrations ranging from 10 µM to 100 µM; (b) Measurement of percentage of viability of HEK-293 cells incubated with compound **6** at various concentrations ranging from 10 µM to 100 µM. Statistical analysis has been done by One-way ANOVA followed by Tukey's test where * denotes a significant difference ($p<0.05$).

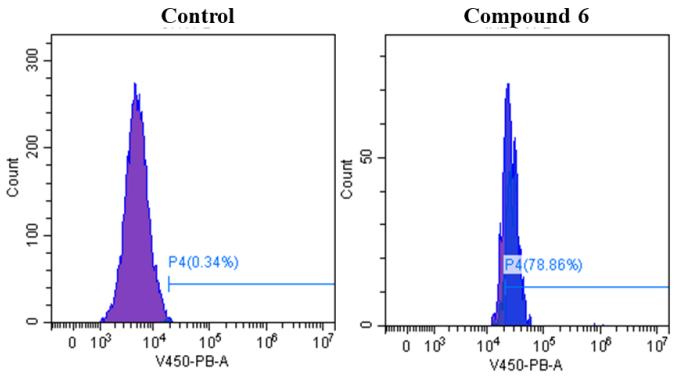

Figure 3.5. Average fluorescence intensity of compound **6** with respect to control determined through flow cytometry in MCF-7 cell lines after 30 minutes of incubation at 20 µM concentration.

3.2. Coumarin-Fused-Azacyclic Group: Application in the Synthesis of Turn-On Fluorescent Probe for Hydrogen Peroxide Detection

3.2.1. Rationale for synthesis of H_2O_2-detecting probe

Selective detection of H_2O_2, specifically among various other ROS, is crucial as it is indicative of cellular oxidative stress and can trigger cell apoptosis at elevated levels. H_2O_2 is a by-product of oxidase enzyme-catalyzed biochemical reactions involved in cellular metabolism and maintenance of cellular homeostasis. Consequentially, abnormal levels of H_2O_2 can be indicative of a multitude of diseases, such as Alzheimer's disease, inflammation, cardiovascular disease, and cancer.[11–15] Therefore, there is an urgent need for fluorescent tools to detect H_2O_2 with high sensitivity. Seeing the excellent potential of compound **6** as the most luminous fluorophore in the azacoumarin series, we constructed a peroxide-susceptible probe (**PYCB**) from compound **6** using carboxy benzyl boronic pinacol ester as the H_2O_2 response unit (figure 3.6).

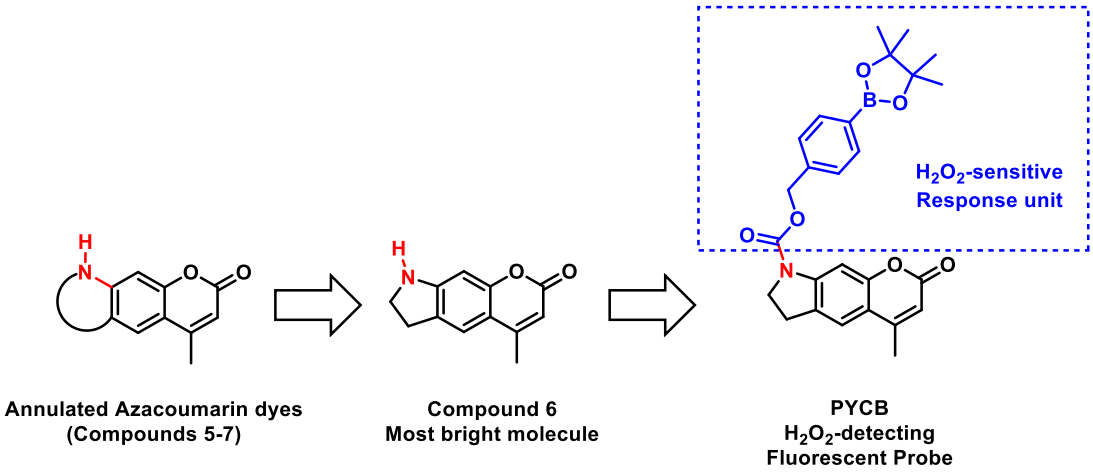

Figure 3.6. The design strategy of azacoumarin-based H_2O_2-susceptible fluorescent probe (**PYCB**).

3.2.2. Results and Discussion

3.2.2.1. Synthesis of probe

The probe (**PYCB**) was constructed using the following synthetic scheme 3.2. Further, its detection mechanism can be demonstrated with the help of figure 3.7. The free NH-group of dye **6** is quenched by the carboxy benzyl boronic pinacol ester, resulting in the attenuation of its fluorescence. Previous literature demonstrates that H_2O_2 definitively oxidizes the phenylboronic ester into a phenol group, initiating self-immolation as *p*-quinone methide via 1,6-elimination and subsequent decarboxylation, effectively eliminating the quencher. This unequivocally leads to the restoration of the fluorescence of the parent fluorophore. [16,17]

Scheme 3.2. Synthesis of azacoumarin-based H_2O_2-susceptible fluorescent probe PYCB from compound 6.

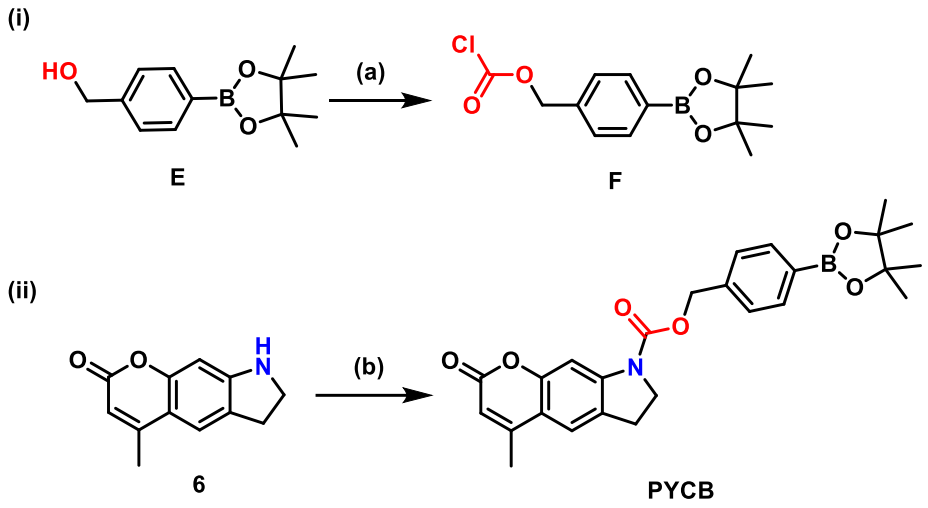

[a]**Reagents and Conditions:** (a) (4-(4,4,5,5-tetramethyl-1,3,2-dioxaborolan-2-yl)phenyl)methanol (**E**, 2.13 mmol), Triphosgene (2 equiv.), Na_2CO_3 (10 equiv.), Toluene, 0 °C to rt, 6h, 90%. (b) **6** (1 mmol), **F** (0.67 equiv.), THF, reflux, overnight, 72%.

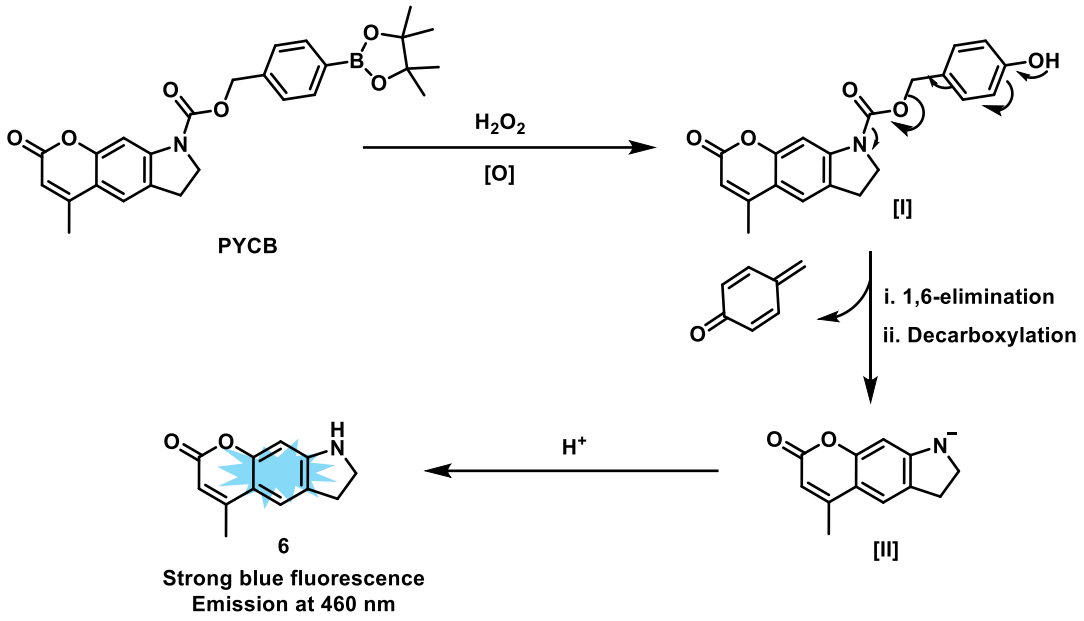

Figure 3.7. Proposed Mechanism for Detection of H_2O_2 by **PYCB.**

3.2.2.2. UV- VIS characterization of probe PYCB in response to H_2O_2

With the desired chemosensor in hand, we then evaluated the spectral response of **PYCB**. The absorption spectrum of probe **PYCB** in PBS shows an absorption band at 263 nm (figure 3.8a). Following the addition of H_2O_2 to the PBS solution **PYCB**, the band centred at 263 nm was substantially suppressed, accompanied by the emergence of a peak at 360 nm, a distinctive characteristic of the parent fluorophore **6**. Introduction of peroxide caused a noticeable color transformation from colorless to pale yellow was visible to the naked eye (figure 3.8a inset). The fluorescence spectrum of PYCB in PBS exhibits a weak fluorescence emission at 460 nm when excited at 350 nm (figure 3.8b). However, upon the addition of H_2O_2, the emission peak at 460 nm experiences a substantial enhancement, emitting a vivid blue fluorescent light (figure 3.8b inset), creating a "turn-on" response to H_2O_2. This signifies the cleavage of **PYCB** in response to H_2O_2 releasing the parent fluorophore **6** which displays an emission maximum at 460 nm.

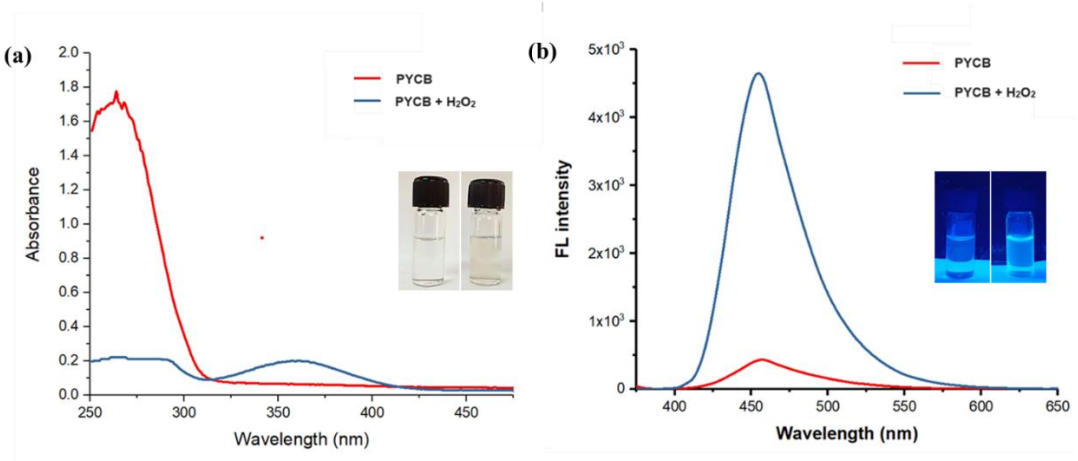

Figure 3.8. (a) UV-vis absorption and (b) fluorescence emission spectra of PYCB (2 μM) in 25 mM PBS mixed with DMSO in a ratio of 8:2 (pH 7.4), before and after the addition of H_2O_2 (5 μM in PBS) (λ_{ex}: 350 nm).

3.2.2.3. Concentration and Time-based Responses of PYCB towards H_2O_2

The fluorescence intensity of **PYCB** increased gradually with the rising concentration of H_2O_2 (figure 3.9a). Additionally, the fluorescence intensity demonstrated a good linear response to H_2O_2 between 5-100 μM (figure 3.9b), with a correlation coefficient of 0.9935 and a detection limit (LOD) of 0.385 μM (calculated using the formula LOD = 3δ/K, where δ is the standard deviation of blank measurements and K is the slope of the plot of fluorescence intensity vs the sample concentration). The sensitivity of the probe reached maximum saturation at an H_2O_2 concentration of 100 μM, beyond which the fluorescence intensity declined rapidly. The time-based response of probe **PYCB** to H_2O_2 was determined by observing the time-dependent variation in its fluorescence intensity when incubated with H_2O_2 (figure 3.9c). The study showed a significant enhancement in fluorescence intensity at 460 nm within 15 minutes of H_2O_2 addition, with the response reaching equilibrium after approximately 2 hours (as shown in Fig. 3.9d). A time-based study of the response of **PYCB** to variable concentrations of H_2O_2

(5-100 μM) also indicates saturation of the probe's response to increasing concentrations of H_2O_2 at about 2h (figure 3.10).

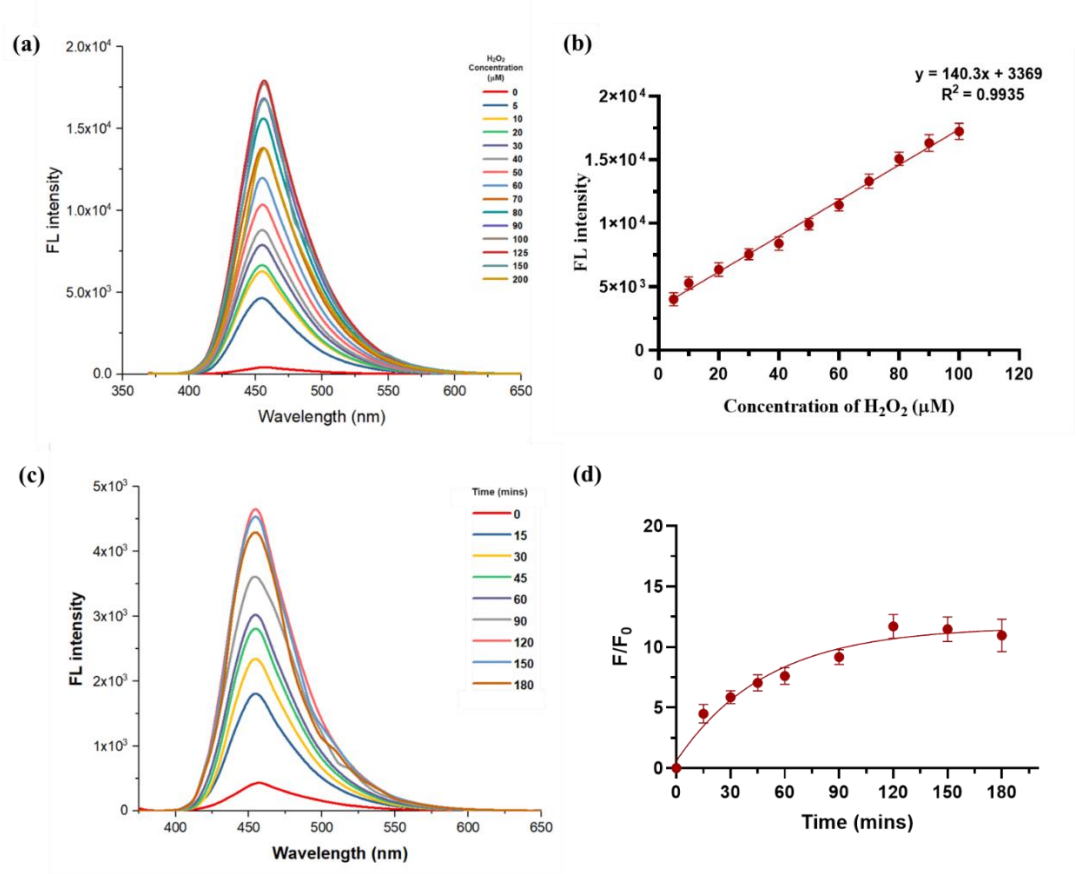

Figure 3.9. (a) Fluorescence responses of PYCB (2 μM) to various concentrations of H_2O_2 (0-200 μM); (b) The linear correlation between the fluorescence intensity at 460 nm and H_2O_2 concentration (5-100 μM); (c) Time-dependent fluorescence response of PYCB (2 μM) to H_2O_2 (5 μM); (d) Total time of response of PYCB to H_2O_2 (5 μM) at 460 nm. (λ_{ex}: 350 nm).

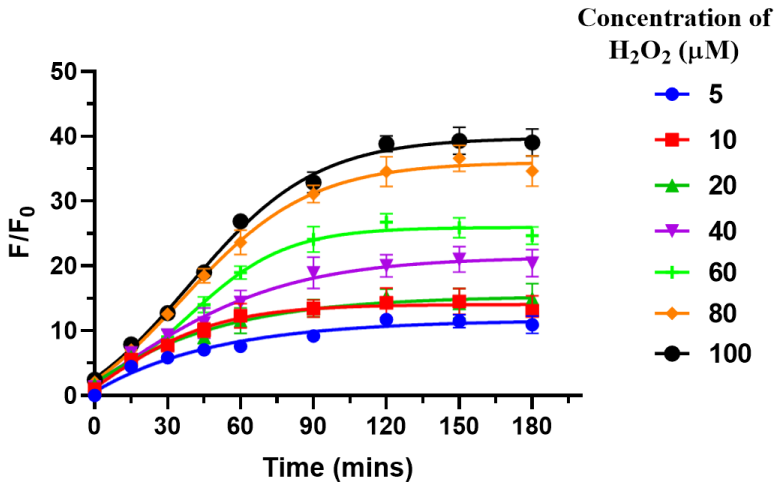

Figure 3.10. Time-based response of PYCB (2 μM) to increasing concentrations of H_2O_2 (5-100 μM) at 460 nm. (λ_{ex}: 350 nm) over a total time period of 3 h where the probe reaches maximum equilibrium at about 2 h in the presence of H_2O_2 at all possible concentrations.

3.2.2.4. pH Stability and Selectivity of PYCB

We thoroughly investigated the pH stability of the probe. **PYCB** demonstrated significant stability in the pH range between 2-8 (figure 3.11a), indicating its strong potential for use in physiological applications. The selectivity study of PYCB towards H_2O_2 was conducted in the presence of various interfering species, such as ions (Na^+, K^+, Fe^{3+}, Cl^-, HCO_3^-, etc.), amino acids (Glu, Cys, GSH), ROS ($ONOO^-$, ClO^-, •NO, TBHP, etc.). As illustrated in figure 3.11b, the probe displayed negligible fluorescence response in the presence of ions and amino acids. However, slight responses have been observed in the presence of most of the ROS, but not as intense as the emission obtained in case of H_2O_2, which exhibited nearly a 12-fold enhancement of the emission compared to the free probe **PYCB**.

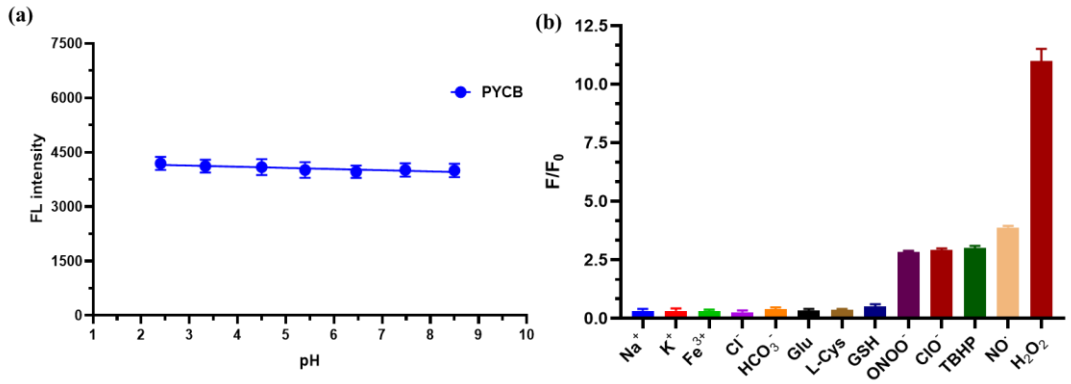

Figure 3.11. (a) Evaluation of the stability of probe **PYCB** (10 μM) to change in pH (2-8) at λ_{em} = 460 nm (λ_{ex}: 350 nm); (b) Fluorescence response of **PYCB** (2 μM) to various competing species (5 μM) and H_2O_2 (5 μM) (λ_{ex}: 350 nm; λ_{em} = 460 nm).

3.2.2.5. Biocompatibility and *In vitro* Cellular Imaging of PYCB

Taking into account the sensitivity and selectivity towards H_2O_2 and stability in variable pH ranges, probe **PYCB** was subjected to detection and imaging of H_2O_2 in living cells. Prior to this, the biocompatibility of the probe was evaluated in breast cancer (MCF-7) cell lines using MTT assay technique. The relative growth rate of MCF-7 cells incubated with **PYCB** in concentrations ranging from 2.5 to 100 μM for 24 h was detected. As shown in figure 3.12, the percentage of cell viability remained above 90% at PYCB concentrations up to 75 μM, demonstrating good biocompatibility and minimal cytotoxicity of the probe within this concentration range and is safe to be used in living systems. Thus, it was taken forward to subsequent fluorescence imaging in cells.

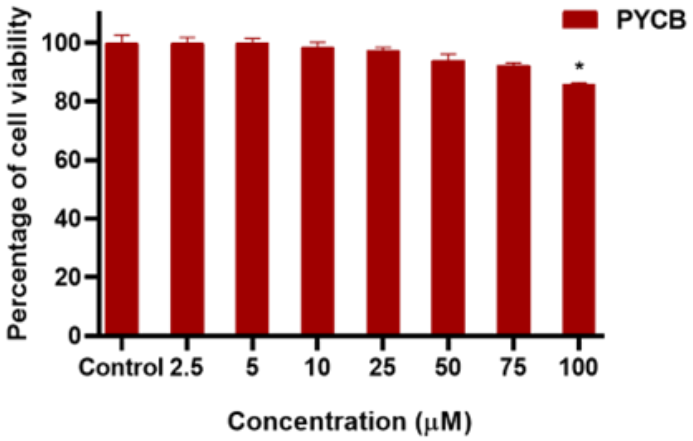

Figure 3.12. Measurement of percentage of viability of MCF-7 cells incubated with probe **PYCB** at various concentrations ranging from 2.5 μM to 100 μM. Statistical analysis has been done by One-way ANOVA followed by Tukey's test where * denotes a significant difference ($p<0.05$).

To conduct fluorescence imaging of the probe, MCF-7 cells were first incubated with the probe **PYCB** (2 μM) and were then exposed to two different concentrations of exogenous H_2O_2 - a lower concentration (10 μM) and a higher concentration (50 μM) in DMEM medium (figure 3.13). After this, the cells were again incubated for 2 hours at 37°C and then washed with PBS. After treating with H_2O_2, the cells clearly displayed bright fluorescence in the blue channel (λ_{abs}: 357/44 nm and λ_{em}: 447/60 nm). These findings strongly support the cell permeability and hydrogen peroxide imaging capabilities of **PYCB** in both higher and lower concentrations within living cells. As observed in the image, cells treated with higher peroxide concentration showed much greater fluorescence emission compared to those treated with lower concentration, indicating a concentration-dependent response of the probe to H_2O_2 in cells. When the probe-treated cells were incubated with exogenous H_2O_2 and *N*-acetylcysteine (NAC), a widely recognized peroxide inhibitor, the blue fluorescence became minimal, clearly demonstrating the susceptibility of the probe to H_2O_2.

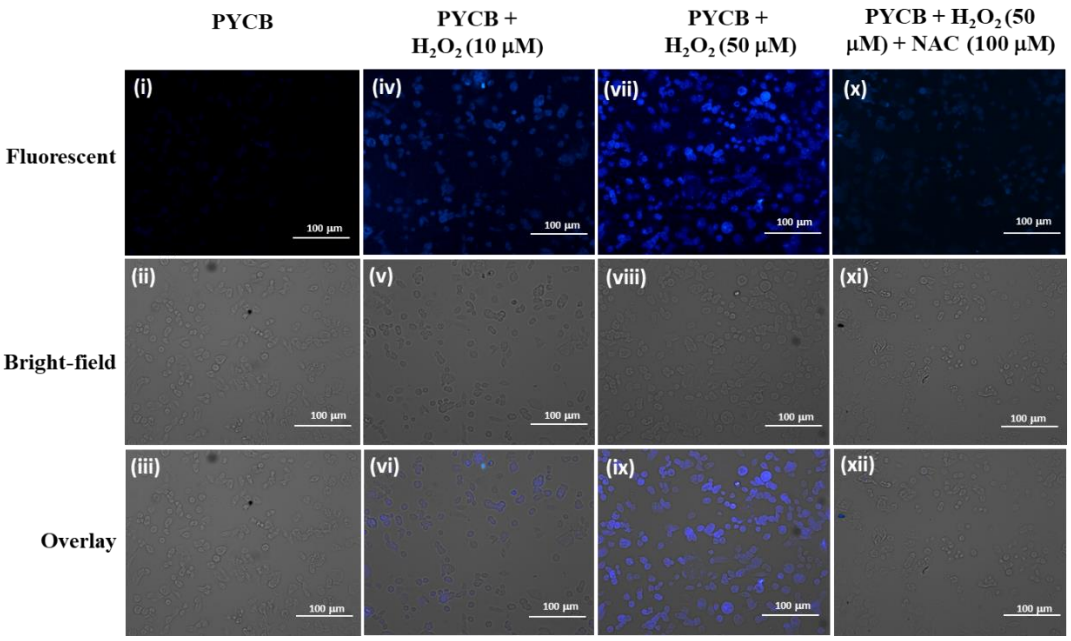

Figure 3.13. Fluorescent, bright-field and merged images of MCF-7 cells treated with probe **PYCB** in absence and presence of exogenous H_2O_2 as well as inhibitor NAC; (i-iii) Cells were treated with probe **PYCB** (2 μM) for 1h, (iv-vi) Cells were treated with probe **PYCB** (2 μM) for 1h, followed by incubation with H_2O_2 (10 μM) for 2 h, (vii-ix) Cells were treated with probe **PYCB** (2 μM) for 1h, followed by incubation with H_2O_2 (50 μM) for 2 h, (x-xii) Cells were treated with probe **PYCB** (2 μM) for 1h, followed by incubation with H_2O_2 (50 μM) and NAC (100 μM) for 2 h. The excitation wavelength was 357/44 nm, and the emission was collected at 447/60 nm. Scale bar = 100 μm.

3.3. Conclusion

In summary, we explored the photophysical properties of azacoumarin fluorophores (**5-7**) and established that dihydropyrrolo-4-methylcoumarin (**6**) possesses the highest brightness. Our extensive investigations demonstrated that compound **6** exhibits exceptional photostability, decent pH stability, good cell permeability, and substantial biocompatibility in both cancer and normal cell lines, in addition to excellent brightness. It also features a free nitrogen centre for the attachment of the response unit. As a result, we were driven to develop a **6**-conjugated

boronic pinacol ester-based probe (**PYCB**) for the detection of H_2O_2. The probe executed good sensitivity and selectivity to H_2O_2 within a concentration range of 5-100 μM, along with a detection limit of 0.385 μM. Moreover, it displayed a time-dependent response to H_2O_2 for approximately 2 h and demonstrated remarkable stability within the pH range of 2-8. Furthermore, the MTT assay showed good biocompatibility of probe **PYCB** in MCF-7 breast cancer cell lines. Fluorescence imaging in MCF-7 cells depicted an increase in the blue fluorescence emission intensity from probe-treated cells, further incubated with both lower and higher peroxide concentrations. This work offers a highly promising strategy for researchers to delve further into the possibilities presented by azacoumarin-based fluorescent probes.

3.4. Experimental Section

3.4.1. Materials and methods

All chemicals were purchased from Sigma-Aldrich, TCI Chemicals, SRL Chemicals, and Avra and used as received. Molychem silica gel (60-120 mesh) was used for column chromatography, and thin-layer chromatography was performed on Merck pre-coated silica gel 60-F254 plates. All other chemicals and solvents were obtained from commercial sources and purified using standard methods. The ^{1}H NMR and ^{13}C NMR spectra were recorded on Bruker-Advance 500 and 600 MHz spectrometers. Chemical shifts (δ) are reported in parts per million (ppm), using TMS (δ = 0) as an internal standard and $CDCl_3$ as NMR solvents. The mass spectrum of the compounds has been obtained by Waters Q-ToF Premier Mass Spectrometer. UV absorbance was measured on an Agilent Cary UV 60 UV-visible spectrophotometer. Fluorescence data were recorded on a Molecular Devices SpectraMax M5 multimode plate reader. Solvents used for absorption and emission spectra of azacoumarins: dimethylsulfoxide (DMSO), dichloromethane (DCM), methanol (MeOH) and phosphate-buffered saline (PBS, 1X) (SRL Chemicals). GraphPad Prism ver. 7.0a (GraphPad Software, Inc.) and Origin2017

softwares were used to analyze data and generate graphs. MCF-7 breast cancer cell lines and HEK-293 normal cell lines were secured from the National Centre for Cell Science (NCCS), Pune, India. Cells were cultured in DMEM (Dulbecco's modified eagle's medium), supplemented with 10% FBS (Gibco, Thermo Scientific, Waltham, MA, USA) and 1% anti-biotic anti-mitotic solution (Himedia, Mumbai, India) (10,000 U Penicillin, 10 mg streptomycin, 25 µg Amphotericin B per ml) and grown at 37°C temperature in a humidified incubator (Heracell VIOS 160i, ThermoFisher. MA, USA). 3-(4,5-dimethylthiazol-2-yl)-2,5-diphenyltetrazolium bromide (MTT), and Fetal bovine serum (FBS) were procured from Thermo Scientific, Waltham, MA, USA.

3.4.2. Photophysical Characterization of compounds 5, 5a, 6 and 7

Maximum absorption wavelengths (λ_{abs}) of all the compounds were recorded using Agilent Cary UV 60 UV–Visible Spectrophotometer. Molar absorption coefficients (ε) were quantified using solutions of compounds **5, 5a, 6** and **7** at concentrations ranging between 10^{-6} - 10^{-5} M in PBS (1X) by direct application of the Beer-Lambert's law. The compound stock solutions were prepared using DMSO (2 mL) and then diluted with PBS (upto 100 mL). Maximum emission wavelengths (λ_{em}) were recorded on a Horiba Scientific FluoroMax-4. λ_{abs} and λ_{em} were recorded in three solvents, namely, Dichloromethane (DCM), Methanol (MeOH) and phosphate buffered saline [PBS, pH = 7.4] (SRL Chemicals) (Supporting information, Table S1). All measurements were taken at ambient temperature (22 ± 2 °C) using 1-cm path length, 4 mL quartz cuvettes. GraphPad Prism ver. 7.0a (GraphPad Software, Inc.) and Origin2017 softwares were used to analyze all the data and generate the corresponding graphs. The spectral data have been normalized for better understanding.

3.4.3. Quantum Yield (φ_f) Measurement

For quantum yield measurement, the compounds (**5, 5a, 6** and **7**) were dissolved in DMSO and PBS mixture (in the ratio of 2:8 v/v) to prepare their respective stock solutions. Next, 3 mL of each sample solution was taken in a 1 cm quartz cuvette and their absorbance values were measured and adjusted between 0.07 to 0.09. After that, five serial dilutions from this 3 mL volume were prepared, and their corresponding absorbance and emission wavelength values were measured. The area of the obtained fluorescence intensity was plotted against their corresponding absorbance intensities in a graph to generate the slope of individual linear equations. The quantum yield of each sample was then calculated using the formula mentioned below, with compound **2a** as the reference standard.

$$\mathbf{Q_f = Q(r) \times (m/m_r) \times (n^2/n_r)}$$

Q(r) = absolute quantum yield of **2a** in PBS

m and m_r = equation slopes derived from the plots of Absorbance vs Area of Fluorescence of the sample and reference **2a,**

n and n_r = refractive indices of the solvents dissolving the test compounds and reference compound, respectively.

3.4.4. pH stability study

For the pH stability study, the buffers having pH ranges 4-8 (4.80, 5.70, 6.64 and 7.48) were prepared using deionized water following standard protocol and freshly used. Compound **6** in a fixed concentration was placed in each buffer system and incubated for 30 mins at 37 ^oC before measuring the fluorescence intensities.

3.4.5. Photostability study

For photostability tests, compound **6,** reference compound **2a** and standard cell labeling dye, **coumarin 6,** were dissolved in DMSO:PBS mixture (in 2:8 v/v ratio) in separate vials, each containing an equimolar concentration of the compounds and placed under continuous irradiation with a 500W tungsten lamp emitting white light. Their emission intensities were then measured from 0 to 360 minutes of irradiation, and the obtained fluorescence intensities were plotted into a curve against time.

3.4.6. *In vitro* cytotoxicity testing of compound 6 using MTT assay

Cytotoxicity of compound **6** against the MCF-7 cancer cell line was analyzed in a 96-well cell culture plate, which contained 1×10^4 cells/well. The cells were evenly distributed onto the entire plate, with each well containing 100 µl of the complete culture medium. The culture plate was then placed in a CO_2 incubator with 5% CO_2 at 37°C for 24 h to allow cell adherence. After 24 h of incubation, the media was aspirated, and fresh media was added comprising of compound **6** at different concentrations within a range of 10 - 100 µM and incubated for another 24 h. After the completion of treatment, media was aspirated, and fresh media (100 µL) containing 500 µg/mL of MTT (3-(4,5-dimethylthiazol-2-yl)-2,5-diphenyltetrazolium bromide) was added to each well and incubated for an additional 3 h at 37°C. The MTT-containing media was then aspirated, followed by the addition of 100 µL of DMSO in each well and subsequent incubation for another 30 mins to dissolve the purple-colored formazan precipitate. The plates were incubated for the next 10 mins with gentle shaking. The optical density of each well was measured at 570 nm using a Bio-Tek microplate reader. A similar protocol was followed for non-cancer HEK-293 cells.

3.4.7. Intracellular uptake assay of compound 6

The MCF-7 cells were seeded in Petri dishes at a density of 5 x 10^5 cells/well and incubated for 24 h in a CO_2 incubator with 5% CO_2 at 37°C to allow cell adherence. After 24 h, the media was aspirated, and the cells were trypsinized and collected, followed by treatment with 500 µl of compound **6** (20 µM). It was then incubated for 30 mins. After incubation, the cells were harvested using 1 mM EDTA in PBS and processed further for experimentation through flow cytometry (CytoFlex LX, Beckman coulter, MA, USA) for the measurement of fluorescence intensities. The experiment was performed in triplicate.

3.4.8. UV-VIS and fluorescence measurements of probe PYCB

The stock solution of probe **PYCB** (100 µM) was made in 25 mM PBS mixed with DMSO in a ratio of 8:2 (pH 7.4). It was then diluted to 2 µM concentration using PBS and used freshly. The stock solution of H_2O_2 (10 mM) was prepared in PBS and then diluted to serial concentrations ranging between 5 – 200 µM and used freshly. The absorption and emission wavelengths of the resultant solution of the probe were measured in the absence and in the presence of H_2O_2 (5 µM solution in PBS) and plotted into graphs. For pH stability study, the buffers having pH ranges 2-8 (2.40, 3.33, 4.50, 5.40, 6.46, 7.48, and 8.5) were prepared using deionized water following standard protocol and freshly used. Probe **PYCB** (10 µM) was placed in each buffer system and incubated for 30 mins at 37 ºC before measuring the fluorescence intensities. Stock solutions (100 mM) of Na^+, K^+, Fe^{3+}, Cl^-, HCO_3^-, Cys, and GSH were prepared respectively in deionized water and used freshly. Stock solutions (100 µM) of HOONO, HClO, H_2O_2, TBHP and *t*BuNO (NO·) were prepared immediately before use. Fluorescence spectra were obtained 90 mins after mixing at 37 ºC.

3.4.9. *In vitro* cytotoxicity testing of PYCB using MTT assay

Cytotoxicity of probe **PYCB** against MCF-7 cell lines was analyzed in a 96-well cell culture plate, which contained 1 × 10^4 cells/well. The cells were distributed such that each well contained 100 μL of the complete culture medium. The culture plate was then placed in a CO_2 incubator with 5% CO_2 at 37°C for 24 h to allow cell adherence. After 24 h of incubation, the media was aspirated, and fresh media was added comprising of probe **PYCB** at different concentrations within a range of 2.5 - 100 μM and incubated for another 24h. After 24 h, media was aspirated, and fresh media (100 μL) containing 500 μg/mL of MTT (3-(4,5-dimethylthiazol-2-yl)-2,5-diphenyltetrazolium bromide) was added to each well and incubated for an additional 3h at 37°C. The MTT-containing media was then aspirated, and 100 μL of DMSO was added to each well and subsequently incubated for another 30 mins to dissolve the formazan precipitate. The plate was incubated for the next 10 mins with gentle shaking. The optical density of each well was measured at 570 nm using a Bio-Tek microplate reader.

3.4.10. Fluorescence imaging of PYCB-treated MCF-7 cells

MCF-7 cells were seeded in a chambered well plate at 3 x 10^4 cells/well density and incubated overnight in a CO_2 incubator with 5% CO_2 at 37°C to obtain cell adherence. After 24 h of incubation, the media was aspirated, and fresh media was added containing 2 μM **PYCB** for 1 h, followed by incubation with H_2O_2 (10 μM and 50 μM) separately for another 2 h. Then, another group MCF-7 cells pre-treated with probe **PYCB** (2 μM), were incubated with H_2O_2 (50 μM) and *N*-Acetylcysteine (100 μM) for another 2 h. After completion of treatment, cells were washed with cold PBS three times, and images were captured using an inverted fluorescence microscope (Olympus BX53, Tokyo, Japan) in the blue channel (λ_{abs}: 357/44 nm and λ_{em}: 447/60 nm) at 400 X magnification.

3.4.11. Synthetic Procedures and Spectral Data

3.4.11.1. Procedure for the synthesis of 7-(azetidin-1-yl)-4-methyl-2H-chromen-2-one (2a).

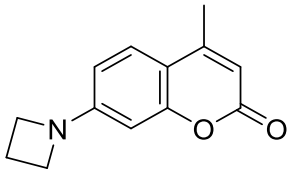

A round bottom flask was charged with 4-methyl-7-nonafluorobutylsulfonyloxy coumarin (1 mmol, 500 mg, 1equiv.), azetidine (2 mmol), tris(dibenzylideneacetone)palladium (5 mol %), xantphos (10 mol %), caesium carbonate (2 mmol), TBAF.$3H_2O$ (1 mmol), and dioxane (4.0 mL) under argon. The resulting solution was heated at 100 ◦C with rapid stirring for 12 h. The reaction mixture was allowed to cool to room temperature and then diluted with water (20 mL) and extracted with ethyl acetate (25 mL × 3). After drying with anhydrous Na_2SO_4, the organic phase was evaporated to dryness and purified by column chromatography using 20% ethyl acetate: hexane. **2a** was obtained as a brownish-yellow solid with 88% yield. ^{1}H NMR (500 MHz, $CDCl_3$) δ 7.39 (d, *J* = 8.5 Hz, 1H), 6.32 (dd, *J* = 2.0 Hz, 2.5 Hz, 1H), 6.22 (d, *J* = 1.8 Hz, 1H), 5.98 (d, J = 1Hz, 1H), 4.00 (t, *J* = 7.5 Hz, 4H), 2.47–2.42 (m, 2H), 2.35 (d, *J* = 1 Hz, 3H). ^{13}C NMR (150 MHz, $CDCl_3$) δ 162.0, 155.6, 154.0, 153.0, 125.4, 110.3, 109.4, 107.7, 97.1, 51.8, 18.6, 16.5. HRMS (ESI) m/ z calculated for $C_{13}H_{13}O_2N$ $[M + H]^+$ calculated as 216.1019, found 216.1039. [18]

3.4.11.2. Procedure for the synthesis of 4-methyl-6,7,8,9-tetrahydro-2H-pyrano[3,2-g]quinolin-2-one (5).

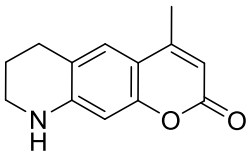

1,2,3,4-tetrahydroquinolin-7-ol (**A**, 2.01 mmol, 300 mg, 1 equiv.) was dissolved in ethanol (2mL) in a round-bottomed flask of 25 mL capacity. Then zinc chloride (3.015 mmol, 1.5 equiv.) was added to the slurry and stirred for 5 mins. Ethyl acetoacetate (2.41 mmol, 1.2 equiv.) was then added to the vessel and the reaction mixture was refluxed at 85 – 90 ºC for 16 h to yield the condensation product.[7] After cooling the reaction mixture, the solvent was evaporated *in vacuo* and the crude mixture was then diluted with water (10 mL) and extracted with ethyl acetate (15 mL×3). After drying with anhydrous Na_2SO_4, the organic phase was evaporated to dryness and the compound was purified by column chromatography using 50% ethyl acetate:hexane. Compound **5** was obtained as bluish-green solid with 75 % yield. ^{1}H NMR (600 MHz, $CDCl_3$) δ 7.02 (s, 1H), 6.32 (s, 1H), 5.85 (s, 1H), 4.61 (s, 1H, NH), 3.30 (t, J = 5.5 Hz, 2H), 2.71 (t, J = 6.0 Hz, 2H), 2.24 (s, 3H) 1.87 (quint, J = 6.0 Hz, 2H). ^{13}C NMR (150 MHz, $CDCl_3$) δ 161.3, 153.1, 152.0, 147.3, 123.7, 117.0, 109.0, 107.7, 98.1, 40.5, 25.8, 20.4, 17.5. HRMS (ESI) m/z calculated for $C_{13}H_{23}NO_2$ $[M + H]^+$ calculated as 216.1019, found 216.1017.

3.4.11.3. Procedure for the synthesis of 4,9-dimethyl-6,7,8,9-tetrahydro-2H-pyrano[3,2-g]quinolin-2-one (5a).

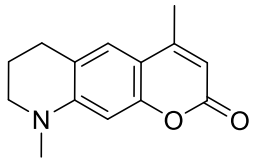

5 (0.96 mmol, 206 mg, 1 equiv.) and potassium carbonate (K_2CO_3) were dissolved in acetonitrile (ACN, 2 mL) in a round-bottomed flask of 25 mL capacity and stirred for 30 mins at room temperature. [7] Then, methyl iodide (1.5 equiv.) was dissolved in ACN (1 ml), added dropwise to the slurry and stirred at 65 ºC for 6 h to obtain the methylated derivative (**5a**). After cooling the reaction mixture, the solvent was evaporated *in vacuo,* and the crude mixture was then diluted with water (10 mL) and extracted with ethyl acetate (15 mL×3). After drying with

anhydrous Na_2SO_4, the organic phase was evaporated to dryness, and the compound was purified by column chromatography using 35% ethyl acetate:hexane. Compound **5a** was obtained as a yellowish-green solid with a 50 % yield. ^{1}H NMR (600 MHz, $CDCl_3$) δ 7.00 (s, 1H), 6.30 (s, 1H), 5.85 (s, 1H), 3.28 (t, *J* = 6.6 Hz, 2H), 2.88 (s, 3H), 2.70 (t, *J* = 6.0 Hz, 2H), 2.24 (s, 3H) 1.87 (quint, *J* = 6.0 Hz, 2H). ^{13}C NMR (150 MHz, $CDCl_3$) δ 162.4, 154.7, 152.9, 149.3, 123.6, 119.4, 109.0, 108.6, 96.6, 50.7, 38.8, 27.5, 21.9, 18.5. HRMS (ESI) m/z calculated for $C_{14}H_{15}NO_2$ $[M + H]^+$ calculated as 230.1176, found 230.1169.

3.4.11.4. Procedure for the synthesis of 4-methyl-7,8-dihydropyrano[3,2-f]indol-2(6*H*)-one (6).

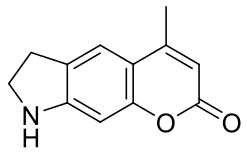

Indole-6-ol (**B**) was converted to indoline-6-ol using literature reference. [9,19] Indolin-6-ol (**C**, 2.22 mmol, 300 mg, 1 equiv.) was dissolved in ethanol (2mL) along with zinc chloride (3.33 mmol, 1.5 equiv.) in a round-bottomed flask of 25 mL capacity and stirred for 5 mins. Ethyl acetoacetate (2.67 mmol, 1.2 equiv.) was then added to the vessel, and the reaction mixture was refluxed at 85 – 90 °C for 6 h to yield the condensation product. After cooling the reaction mixture, the solvent was evaporated *in vacuo* and the crude mixture was then diluted with water (10 mL) and extracted with ethyl acetate (15 mL×3). After drying with anhydrous Na_2SO_4, the organic phase was evaporated to dryness and the compound was purified by column chromatography using 50 % ethyl acetate:hexane. Compound **6** was obtained as brown solid with 75 % yield. ^{1}H NMR (600 MHz, $CDCl_3$) δ 7.14 (s, 1H), 6.36 (s, 1H), 5.86 (s, 1H), 3.61 (t, *J* = 8.4 Hz, 2H), 3.00 ((t, *J* = 8.4 Hz, 2H), 2.24 (s, 3H). ^{13}C NMR (150 MHz, $CDCl_3$) δ 161.3, 154.5, 154.4, 152.3, 125.3, 118.7, 110.0, 107.7, 94.3, 46.4, 27.4, 17.8. HRMS (ESI) m/z calculated for $C_{12}H_{11}NO_2$ $[M + H]^+$ calculated as 202.0863, found 202.0865.

3.4.11.5. Procedure for the synthesis of 4-methylpyrano[2,3-b]carbazol-2(10*H*)-one (7).

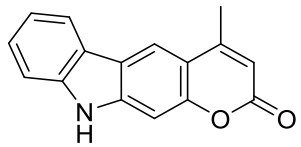

9*H*-carbazol-2-ol (**D**, 1.63 mmol, 300 mg, 1 equiv.) was dissolved in ethanol (2mL) in a round-bottomed flask of 25 mL capacity. Ethyl acetoacetate (1.96 mmol, 1.2 equiv.) was then added to the vessel, and the reaction mixture was kept for stirring. 200 µL of conc. H_2SO_4 was slowly glided through the wall of the flask, and after the complete addition of the acid, the slurry refluxed at 85 – 90 ºC for 16 h.[10] After ensuring the product formation via TLC, the reaction mixture was cooled, and the solvent was evaporated *in vacuo.* The crude mixture was then diluted with water (10 mL) and extracted with ethyl acetate (15 mL×3). After drying with anhydrous Na_2SO_4, the organic phase was evaporated to dryness and the compound was purified by column chromatography using 35% ethyl acetate:hexane. Compound **7** was obtained as a white solid with 55 % yield. ^{1}H NMR (500 MHz, $CDCl_3$) δ 10.87 (s, 1H), 8.21 (s, 1H), 8.07 (d, *J* = 7.0 Hz, 1H), 7.51 – 7.41 (m, 2H), 7.32 (s, 1H), 7.25 – 7.22 (m, 1H), 6.15 (s, 1H), 2.56 (s, 3H). ^{13}C NMR (125 MHz, $CDCl_3$) δ 166.5, 158.5, 157.2, 147.2, 145.9, 131.0, 127.2, 125.6, 124.9, 124.4, 120.7 (d, *J* = 8.75 Hz), 117.5, 116.0, 115.7, 102.4 (d, *J* = 8.75 Hz), 23.9. HRMS (ESI) m/z calculated for $C_{16}H_{11}NO_2$ $[M + H]^+$ calculated as 250.0863, found 250.0859.

3.4.11.6. Procedure for the synthesis of 4-(4,4,5,5-tetramethyl-1,3,2-dioxaborolan-2-yl)benzyl-4-methyl-2-oxo-6,7-dihydropyrano[3,2-f]indole-8(2H)-carboxylate (PYCB).

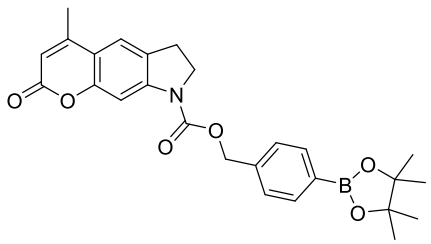

A round-bottomed flask charged with (4-(4,4,5,5-tetramethyl-1,3,2-dioxaborolan-2-yl)phenyl)methanol (**E**, 2.13 mmol, 500 mg, 1 equiv.) and dried Na_2CO_3 (2.9 g, 10 equiv.), dissolved in toluene (2 mL), was kept at 0 ºC on an ice bath. In a glass beaker, crystals of triphosgene (1.2g, 2 equiv.) were dissolved in toluene (2 mL), and this solution was gradually added to the slurry in the round-bottomed flask.[16] After the addition of triphosgene, the reaction vessel was removed from the ice bath and gradually brought to rt. The reaction mixture was then stirred for 6 h at rt. After completion of the reaction, the slurry was diluted with ice-cold water (50 mL) and extracted with ethyl acetate (15 mL x 3). After drying with anhydrous Na_2SO_4, the organic phase was evaporated to dryness, and the compound F was obtained as a faint pink-colored liquid with about 90% yield. Next, the obtained compound **F** (0.67 equiv.) was reacted with compound **6** (1 mmol, 150 mg, 1 equiv.) in THF under reflux conditions overnight. After cooling to rt, the reaction mixture was diluted with water (20 mL) and extracted with ethyl acetate (10 mL x 3). After drying *in vacuo,* the probe **PYCB** was purified via column chromatography using 15% ethyl acetate:hexane and was isolated as a white, flaky solid in 72% yield. ^{1}H NMR (600 MHz, d^6-DMSO) δ 9.30 (s, 1H), 7.70 (d, J = 9 Hz, 2H), 7.43 (d, J = 7.2 Hz, 2H), 6.97 (d, J = 7.8 Hz, 1H), 6.36 (dd, J = 7.8 Hz, 1.8 Hz, 1H), 5.24 (s, 2H), 3.99 (s, 2H), 3.32 (s, 3H), 2.97 (t, J = 7.8 Hz, 2H), 1.29 (s, 12H). ^{13}C NMR (150 MHz, d^6-DMSO) δ 162.05, 157.3, 148.4, 145.2, 139.8, 139.5, 132.0, 130.9, 130.2, 126.2, 114.4, 107.4, 88.9, 71.1, 53.1, 31.3, 29.8. HRMS (ESI) m/z calculated for $C_{26}H_{28}BNO_6$ $[M + H]^+$ calculated as 462.2082, found 462.2075.

3.4.12. References

(1) Grimm, J. B.; Lavis, L. D. Caveat Fluorophore: An Insiders' Guide to Small-Molecule Fluorescent Labels. *Nat. Methods* **2022**, *19* (2), 149–158. https://doi.org/10.1038/s41592-021-01338-6.

(2) Gandioso, A.; Bresolí-Obach, R.; Nin-Hill, A.; Bosch, M.; Palau, M.; Galindo, A.; Contreras, S.; Rovira, A.; Rovira, C.; Nonell, S.; Marchán, V. Redesigning the Coumarin Scaffold into Small Bright Fluorophores with Far-Red to Near-Infrared Emission and Large Stokes Shifts Useful for Cell Imaging. *J. Org. Chem.* **2018**, *83* (3), 1185–1195. https://doi.org/10.1021/acs.joc.7b02660.

(3) Grimm, J. B.; English, B. P.; Chen, J.; Slaughter, J. P.; Zhang, Z.; Revyakin, A.; Patel, R.; Macklin, J. J.; Normanno, D.; Singer, R. H.; Lionnet, T.; Lavis, L. D. A General Method to Improve Fluorophores for Live-Cell and Single-Molecule Microscopy. *Nat. Methods* **2015**, *12* (3), 244–250. https://doi.org/10.1038/nmeth.3256.

(4) Liu, X.; Qiao, Q.; Tian, W.; Liu, W.; Chen, J.; Lang, M. J.; Xu, Z. Aziridinyl Fluorophores Demonstrate Bright Fluorescence and Superior Photostability by Effectively Inhibiting Twisted Intramolecular Charge Transfer. *J. Am. Chem. Soc.* **2016**, *138* (22), 6960–6963. https://doi.org/10.1021/jacs.6b03924.

(5) Zhou, J.; Lin, X.; Ji, X.; Xu, S.; Liu, C.; Dong, X.; Zhao, W. Azetidine-Containing Heterospirocycles Enhance the Performance of Fluorophores. *Org. Lett.* **2020**, *22* (11), 4413–4417. https://doi.org/10.1021/acs.orglett.0c01414.

(6) Indurthi, H. K.; Goswami, P.; Das, S.; Saha, P.; Koch, B.; Sharma, D. K. 7-Azaspiroketal as a Unique and Effective Auxochrome Moiety: Demonstration in a Fluorescent Coumarin Dye and Application in Cell Imaging. *New J. Chem.* **2023**, *47* (47), 21608–21611. https://doi.org/10.1039/D3NJ04934E.

(7) Atkins, R. L.; Bliss, D. E. Substituted Coumarins and Azacoumarins. Synthesis and Fluorescent Properties. *J. Org. Chem.* **1978**, *43* (10), 1975–1980. https://doi.org/10.1021/jo00404a028.

(8) Rodighiero, P.; Chilin, A.; Pastorini, G.; Guiotto, A. Pyrrolocoumarin Derivatives as Potential Photoreagents toward DNA. *J. Heterocycl. Chem.* **1987**, *24* (4), 1041–1043. https://doi.org/10.1002/jhet.5570240426.

(9) Quanten, E.; Adriaens, P.; De Schryver, F. C.; Roelandts, R.; Degreef, H. Photophysical Behaviour of New Pyrrolocoumarin Derivatives. *Photochem. Photobiol.* **1986**, *43* (5), 485–492. https://doi.org/10.1111/j.1751-1097.1986.tb09524.x.

(10) Mihara, J.; Fujimoto, K. Photocrosslinking of DNA Using 4-Methylpyranocarbazole Nucleoside with Thymine Base Selectivity. *Org. Biomol. Chem.* **2021**, *19* (45), 9860–9866. https://doi.org/10.1039/D1OB01621K.

(11) Xu, K.; He, L.; Yang, X.; Yang, Y.; Lin, W. A Ratiometric Fluorescent Hydrogen Peroxide Chemosensor Manipulated by an ICT-Activated FRET Mechanism and Its Bioimaging Application in Living Cells and Zebrafish. *Analyst* **2018**, *143* (15), 3555–3559. https://doi.org/10.1039/C8AN00842F.

(12) Ye, S.; Hu, J. J.; Zhao, Q. A.; Yang, D. Fluorescent Probes for in Vitro and in Vivo Quantification of Hydrogen Peroxide. *Chem. Sci.* **2020**, *11* (44), 11989–11997. https://doi.org/10.1039/D0SC04888G.

(13) Kumar, M.; Kumar, N.; Bhalla, V.; Sharma, P. R.; Qurishi, Y. A Charge Transfer Assisted Fluorescent Probe for Selective Detection of Hydrogen Peroxide among Different Reactive Oxygen Species. *Chem. Commun.* **2012**, *48* (39), 4719–4721. https://doi.org/10.1039/C2CC30932G.

(14) Das, S.; Indurthi, H. K.; Asati, P.; Saha, P.; Sharma, D. K. Benzothiazole Based Fluorescent Probes for the Detection of Biomolecules, Physiological Conditions, and Ions

Responsible for Diseases. *Dyes Pigm.* **2022**, *199*, 110074. https://doi.org/10.1016/j.dyepig.2021.110074.

(15) Das, S.; Indurthi, H. K.; Saha, P.; Sharma, D. K. Coumarin-Based Fluorescent Probes for the Detection of Ions, Biomolecules and Biochemical Species Responsible for Diseases. *Dyes Pigm.* **2024**, *228*, 112257. https://doi.org/10.1016/j.dyepig.2024.112257.

(16) Kim, D.; Kim, G.; Nam, S.-J.; Yin, J.; Yoon, J. Visualization of Endogenous and Exogenous Hydrogen Peroxide Using A Lysosome-Targetable Fluorescent Probe. *Sci. Rep.* **2015**, *5* (1), 8488. https://doi.org/10.1038/srep08488.

(17) Wang, X.; Huang, Y.; Lv, W.; Li, C.; Zeng, W.; Zhang, Y.; Feng, X. A Novel Fluorescent Probe Based on ESIPT and AIE Processes for the Detection of Hydrogen Peroxide and Glucose and Its Application in Nasopharyngeal Carcinoma Imaging. *Anal. Methods* **2017**, *9* (12), 1872–1875. https://doi.org/10.1039/C7AY00167C.

(18) Das, S.; Goswami, P.; Verma, V. K.; Indurthi, H. K.; Kumar, M.; Koch, B.; Sharma, D. K. Rapid Access to 7-Substituted Cycloalkylamino and Alkylamino Analogues of 4-Methylcoumarin Reveals Surprising Emitters. *Dyes Pigm.* **2023**, *217*, 111407. https://doi.org/10.1016/j.dyepig.2023.111407.

(19) Sharma, D. K.; Rah, B.; Lambu, M. R.; Hussain, A.; Yousuf, S. K.; Tripathi, A. K.; Singh, B.; Jamwal, G.; Ahmed, Z.; Chanauria, N.; Nargotra, A.; Goswami, A.; Mukherjee, D. Design and Synthesis of Novel N,N′-Glycoside Derivatives of 3,3′-Diindolylmethanes as Potential Antiproliferative Agents. *Med. Chem. Commun.* **2012**, *3* (9), 1082–1091. https://doi.org/10.1039/C2MD20098H.